UNIVERSITY OF KWAZULU-NATAL ™

INYUVESI YAKWAZULU-NATALI

PREPARATION AND CHARACTERIZATION OF ORGANIC SOLAR CELL

MSc Dissertation

by

July Teboho Bell, BSCA, BSHPH

Under the supervision of

Prof. Genene Tessema Mola

Pietermaritzburg Campus, South Africa

2013

PREPARATION AND CHARACTERIZATION OF ORGANIC SOLAR CELL

MSc Dissertation

by

July Teboho Bell (207509137), BSCA, BSHPH

Under the supervision of

Prof. Genene Tessema Mola

University of KwaZulu-Natal

Pietermaritzburg Campus, South Africa

02 September 2013

Submitted in fulfilment of the academic requirements for the degree of Master of Science in the School of Chemistry and Physics, University of KwaZulu-Natal, Pietermaritzburg.

As the candidate's supervisor I have/have not approved this dissertation for submission.

Signed: _____ Name: _____

Date: _____

Contents

Abstract

Organic molecules based photovoltaic cells were fabricated in an open laboratory conditions without the use of glove box or clean room. Conducting polymers such as P3HT and PCBM were used as a photo-active layer of the devices. We found significant difference in the performance of the devices by employing two laboratory conditions of the polymer solutions. Enhanced current density has been observed from P3HT/PCBM bulkheterojunction solar cell after diluting a well sonicated polymers solution with fresh chloroform solvent. As the result of such current surge in the devices the efficiency rose to more than double compared to those devices without dilution of the P3HT/PCBM solution. An average power conversion efficiency of 4.5% was then recorded from the new preparation condition. This is an encouraging development toward achieving low cost organic photovoltaic devices.

Preface and Declarations

The work described by this dissertation was carried out at the University of KwaZulu-Natal, School of Chemistry and Physics, Pietermaritzburg, from **25 January 2012** until **02 September 2013**, under the supervision of **Prof. Genene Tessema Mola**.

This dissertation is entirely, unless specifically contradicted in the text, the work of the candidate, **July Bell**, has not been previously submitted, in whole or in part, to any other tertiary institution. Where use has been made of the work of others, it is duly acknowledged in the text.

Declaration - Plagiarism

I, _____ declare that

1. The research reported in this dissertation, except where otherwise indicated, is my original research.
2. This dissertation has not been submitted for any degree or examination at any other university.
3. This dissertation does not contain other persons' data, pictures, graphs or other information, unless

   specifically acknowledged as being sources from other persons.
4. This dissertation does not contain other persons' writing, unless specifically acknowledged as being sources from other researchers. Where other written sources have been quoted, then:

   a. Their words have been rewritten but the general information attributed to them has been referenced.
   b. Where their exact words have been used, then their writing has been placed in italics and inside quotation marks, and referenced.

5. This dissertation does not contain, text, graphics or tables copied and pasted from the Internet, unless specifically acknowledged, and the source being detailed in the dissertation and in the References sections.

Signed: _____

Acknowledgements

Firstly, I am ever grateful to God, the Creator and Whom sacrificed His only Son to welcome me back into His Kingdom.
Secondly, I am heartily thankful to my supervisor, Prof. Genene Tessema Mola, whose encouragement, guidance and support throughout the period of my research helping me understand the subject and use of all laboratory equipments better.
Thirdly, I would like to thank, NRF, for awarding me with a Scholarship for all my previous hard-work and to continue doing masters with ease without stressing about money so that I can support my parents and sisters.
Finally, I would like to thank the school of Chemistry and Physics, Electronics and Mechanical Workshop, all Technicians and my family.

July Teboho Bell

02-08-13, University of KwaZulu-Natal, Pietermaritzburg

Chapter 1

Introduction

We live in a society that consumes huge amounts of energy to fulfil our day to day activities that mostly depend on new technologies. The rapid global population growth which aggravates the demand for more energy on one hand, and the dwindling size of fossil fuel on the other raises the need to look for alternative sources of energy. Furthermore, the ever increasing costs of electrical power from conventional energy sources compounded with the diverse effect of fossil fuels on global climate changes become the driving force to shift our energy options to renewable ones.

Solar energy is one of the renewable energy sources which traditionally has been utilised using silicon based solar panels. However, the processing of silicon for the fabrication of solar cells is still very expensive and becomes unaffordable for many. Recently, organic molecules based photovoltaic cells came into picture with the view mainly to reduce the cost of production of the solar cells. Although a few class of organic molecules show encouraging

properties in terms of power conversion and charge transport properties but there are still unresolved issues to compute in the energy market. Several research efforts since the last two decades have produced encouraging results towards the realisation of organic photovoltaic cells (OPV) [1]. OPV has attracted scientific and economic interest triggered by a rapid increase in power conversion efficiency.

The sun is the source of all forms of energy directly and/or indirectly. The energy in the form of electromagnetic radiation coming from the sun first strikes the upper atmosphere before reaching to the surface of the earth. The amount of energy intercepted from the sun at the outer limits of the atmosphere is about 1367 W/m^2 [2]. Among the total solar radiation spectrum often reaching the surface the visible and infrared regions constitute the majority of the emission. Most solar cells currently operate by harvesting the electromagnetic radiation from these two main regions of the solar spectrum.

The conversion of electromagnetic radiation energy into electricity was first noted by the French physicist, Edmund Becquerel, in 1839, who found that certain materials, such as semiconductors, have the ability to produce low voltage and direct current electricity when exposed to light [3]. In the early 20^{th} century, Albert Einstein was able to account for the quantized nature of light in the photoelectric effect experiments for which he earned a Noble prize in 1905. Since then the idea of generating free charge carriers by means of electromagnetic radiation has been used for different purposes such as radiation detectors and solar cells [1].

The working principles of a solar cell can easily be described through the energy band gap theory of semiconductors as well as the theory of Schottky diodes. An incident photon with energy greater than or equal the energy band-gap of the material ($h\nu \geq E_{gap}$) can excite electrons from the valence band to the conduction band which can then contribute to the electrical conduction. The maximum current that can be generated from the material depends on the amount of radiation flux incident on it as well as the energy of the photons. Excess energy of the photons ($h\nu - E_{gap}$) will be lost as heat energy. In the case of inorganic semiconductors, the excitation of an electron to the conduction band results in the creation of a hole in the valence band. The electrons and holes are transported to the opposite face of the semiconductor creating a potential difference which generates electricity [4, 5]. In the case of organic semiconductors (conducting polymers), the mechanisms of charge generation is a bit different. The incident photon first generate a bound electron-hole pair called exciton which eventually dissociates to free charge carriers by external electric field followed by the transport towards the electrodes.

Currently, the renewable energy markets are dominated by the inorganic semiconductor solar cells such as mono-and poly-crystalline silicon. These conventional solar cells can convert as much as 24% of the incoming solar energy which is already close to the theoretically predicted upper limit of 30% [1]. There is clearly the need for low device fabrication costs, rather than higher conversion efficiency in order avail cheap renewable energy. It

is here that the organic photovoltaic cells can actually play a vital role in reducing the device fabrication cost.

This dissertation deals with the preparation and characterization of organic molecules based photovoltaic cells. The advantages of organic molecule (conducting polymers) over the traditional silicon based solar cells are, organic photovoltaic cell can be easily processed using spin coating or doctor blade techniques (wet-possessing) or evaporation through a mask (dry-processing). The photo-active film of organic materials are relatively thin (100 nm thick) and large scale production can be possible by way of screen printing. The energy gap of organic molecules can be fine-tuned to increase the photon harvesting mechanisms of the polymer. Organic polymers are cost-effective, flexible and lightweight [8].

Chapter 2

Theory of Semiconductors

2.1 Semiconductors

Semiconductors are materials that are often used in the fabrication of electronic and optoelectronic devices [9]. Semiconductors are the basic materials for the fabrication of most house hold and work place electronics. Today's life style could not have come to reality without the use of semiconductors. Semiconductors have tremendously contributed to the progress in communication, information technology, computing as well as solar energy conversion. Devices based on semiconductors include transistors, switches, diodes, photovoltaic cells, and detectors etc. These may be used as a single circuit elements or as components of integrated circuits. According to the energy band theory of solids, solids can be classified into metals, semiconductors and insulators based on the magnitude of the energy band gap (E_g). Figure 2.1 shows the energy band diagram of solids consisting of conduction band and valence band. The band gap (E_g) is the difference between the lowest point

of the conduction band edge and the highest point of valence band edge. The free charge carriers available in conduction and valence band are responsible for the electrical conduction of the material. The source of these free charge carriers can either be the thermal excitation of electrons from valence band to conduction band or/and can be impurities origin. A highly purified semi-

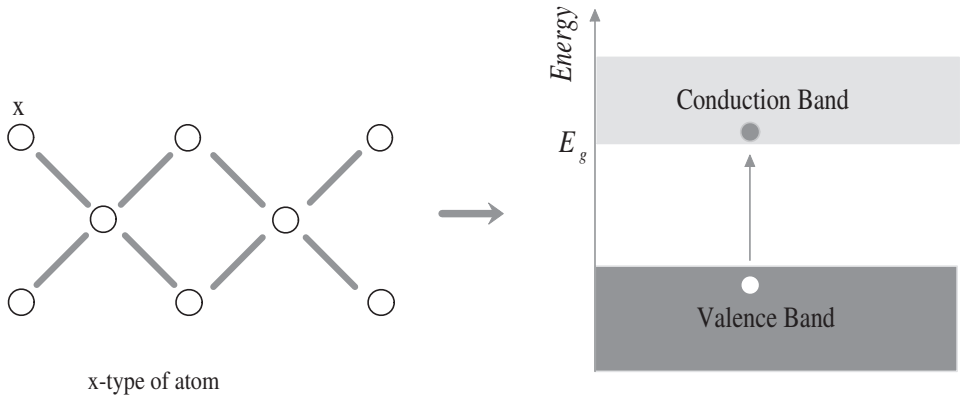

Figure 2.1: Energy band diagram of intrinsic semiconductor.

conductor exhibits intrinsic conductivity, as distinguished from the impurity conductivity of less pure specimens. In the intrinsic temperature range, the electrical properties of a semiconductor are not essentially modified by impurities in the crystal. It is easy to derive the intrinsic concentrations of charge carriers in semiconductors by employing the Fermi-Dirac statistics. Therefore, the intrinsic concentration of carriers in conduction band is given by the relation

$$n = 2(\frac{m_e kT}{2\pi\hbar^2})^{3/2} e^{(E_F - E_c)/kT}. \quad (2.1)$$

Similarly, the intrinsic concentration of hole in the valance band can be written as

$$p = 2(\frac{m_h kT}{2\pi\hbar^2})^{3/2} e^{(E_v - E_F)/kT} \tag{2.2}$$

where m_e and m_h are the effective mass of holes and electrons in the material. In an intrinsic conduction for every electron available in conduction band there will be a hole in the valence band. Therefore, under intrinsic condition n=p;

$$np = n_i^2 \tag{2.3}$$

$$n_i = 2(\frac{kT}{2\pi\hbar^2})^{3/2}(m_e m_h)^{3/4} e^{-(E_g/2kT)}. \tag{2.4}$$

The intrinsic conductivity and intrinsic carrier concentrations are largely controlled by E_g/k_BT, the ratio of the band gap energy to the thermal energy(k_BT). When this ratio is large, the concentration of intrinsic carrier will be low and so is the conductivity. The balance of the charge concentration can be changed by incorporating impurities in the host matrix by the process called **doping**. There are n-type and p-type of doping in semiconductors. When a group-III element of the periodic substitute a silicon atom, for example, the impurity takes an electron from the valence band of silicon to make the bonds with four nearest neighbours of silicon atoms. This process creates an excess hole in the valence band of silicon making the doped silicon as p-type. Similarly, group-V elements in silicon form an n-type silicon. Unlike inorganic semiconductors doping in organic semiconductors

is achieved by adding or subtracting of electrons from the back bone of the polymer chain by the process of oxidation or reduction.

2.2 Metal-Semiconductor Contacts

Metal-semiconductor contact is the most frequently used mechanism in the fabrication of electronic devices and photonic devices. When metals and semiconductors are fused together to form a contact, potential barrier will be created as the result of the difference in the work functions of the two material as well as the potential due to the so called **Schottky effect**. Schottky suggested that the potential barrier at metal-semiconductor contact could arise from stable space charge in the semiconductor-metal interface. This is the initial assumption used to describe the rectifying behaviour of the current across the contacts. Let us first start the discussion by considering the motion of electrons near metal-vacuum interface in which the electrons are emitted from the surface and caught by the applied electric field in vacuum. Figure

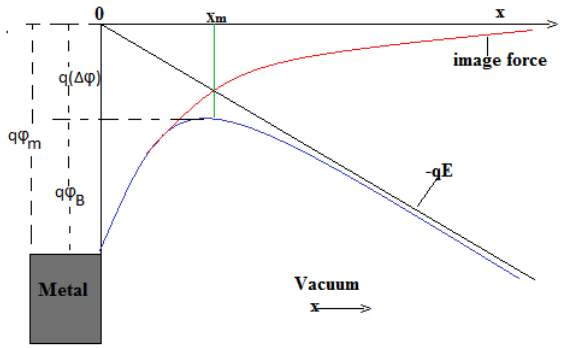

Figure 2.2: Schottky potential barrier at Metal-Semiconductor contact.

2.2 shows the energy diagram for metal-vacuum interface which is in fact can

be used to describe metal-semiconductor as well. In this energy diagram a vacuum level is taken as reference level where the electron is free without any external influence. In a metal-vacuum system the minimum energy necessary for an electron to escape into vacuum from an initial energy at Fermi level is defined in terms of a work function Φ_m. An electron needs to overcome the energy $q\Phi_m$ in order to escape from the surface in the first place. Once the charges are free from the surface then it would be subject to external field **E**. When an electron is at distance x from the metal, a positive charge will be induced on the surface. The force of attraction between the electron and the induced positive charge is equivalent to the force which would exist between the electron and an equal positive charge located at $-x$. This positive charge is referred to as the ""image force"", is given by:

$$F = \frac{-q^2}{4\pi\epsilon_0(2x)^2} \tag{2.5}$$

where ϵ_0 is the permittivity of free space. The work done by an electron in the course of its transfer from infinity to the point x is given by:

$$U(x) = \int_{\infty}^{x} F dx = \frac{-q^2}{16\pi\epsilon_0 x}. \tag{2.6}$$

Equation (2.6) corresponds to the potential energy if an electron at distance x from the metal as shown in Figure 2.2 and is measured downwards from x-axis. When an external field E is applied, the potential energy, V(x) as

function of distance is given by the sum:

$$V(x) = \frac{-q^2}{16\pi\epsilon_0 x} - qEx \tag{2.7}$$

where the field **E** is applied in x-direction. If $E = 0$, then the maximum value of $V(r) = 0$ and occurs at infinite distance from traps. The Schottky barrier lowering $\Delta\phi$, and the location of lowering $x_m = \sqrt{\frac{q}{16\pi\epsilon_0|E|}}$, can be derived from the condition dV(x)/dx = 0. It easy to find:

$$\begin{aligned} \Delta\phi &= \sqrt{\frac{qE}{4\pi\epsilon_0}} \\ &= 2|E|x_m. \end{aligned} \tag{2.8}$$

The lowering of the metal work function by an amount $\Delta\phi$ as the result of ""image force"" and the electric field is called the Schottky effect. This result can be extended to metal-semiconductor interface. However, the field should be replaced by the maximum field at the surface and free-space permittivity ϵ_0 by permittivity of the medium ϵ.

Chapter 3

Charge Transport Properties

3.1 Charge transport theory

The charge transport across two oppositely charged electrodes has been the focus of intense investigation for the past several decades. Starting from simple to the most complex electronic devices, the motion of charges across the electrodes have been an interesting phenomena for science and engineering. The charge transport between electrodes in fact has significant influence on the performance of the device. The earlier studies provided us with a broad look into the picture of charge transport across the electrodes. In 1938 a model was proposed to provide a picture on how an electron traverses between electrodes in semiconductor diode designed to understand the transport between two electrodes.

3.1.1 Current Density Equation

The main mechanisms of the flow of charges across a junction are drift due to applied electric field and diffusion due to charge concentration gradient. Based on the drift and diffusion theory of charges in a device the current equations for negative and positive charge q can be written as

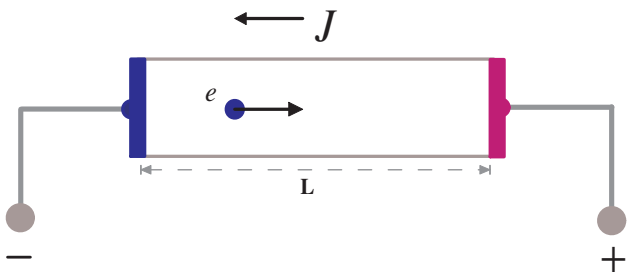

Figure 3.1: A conductor connected to external voltage.

$$J_n = q\mu_n n(x)\overrightarrow{E} + qD_n\frac{dn(x)}{dx} \tag{3.1}$$

$$J_p = q\mu_p p(x)\overrightarrow{E} - qD_p\frac{dp(x)}{dx} \tag{3.2}$$

where $\overrightarrow{E}$ is the applied electric field in the x-direction and $n(x)$ is the density of electrons in the device, $D_i(i = n, p)$ is a diffusion coefficient, $\mu_i(i = n, p)$ is the mobility of the charger carriers. J_n and J_p are the current densities for negative and positive charges, respectively. In the case where the current involves both types of charge carriers in the devices then the total conduction

current can be written as:

$$\overrightarrow{J} = \overrightarrow{J_n} + \overrightarrow{J_p} \tag{3.3}$$

3.1.2 Space Charge Current

Space charge limited regime is characterized by the fact that all traps are filled and the current reached steady state condition. The current density equation describing the steady state condition can be deduced from current equation (for single type of charge carrier), as well as the Poisson equation as:

$$\frac{dJ}{dx} = 0 \tag{3.4}$$

$$J = q\mu_n n(x)\overrightarrow{E}(x) \tag{3.5}$$

$$\frac{dE}{dx} = \frac{q}{\epsilon}n(x) \tag{3.6}$$

where ϵ is the dielectric constant and μ_n is the carrier mobility. From equations 3.4, 3.5 and 3.6 one can write:

$$\frac{d\overrightarrow{E}}{dx} = \frac{J}{\epsilon\mu_n E(x)}. \tag{3.7}$$

After integration and rearrangement one finds the space charge limited current as:

$$J = \frac{9}{8}\epsilon\mu_n\frac{V^2}{L^3}. \tag{3.8}$$

The last equation is known as Mott-Gurney law which holds true for the current density in the absence of traps in the medium. The carrier velocity ν is related to the electric field by:

$$\nu = \mu \mathbf{E} \tag{3.9}$$

$$\nu = \sqrt{\frac{2qV}{m^\star}} \tag{3.10}$$

in the velocity saturated regime:

$$J = \frac{2\epsilon_s \nu_s V}{L^2} \tag{3.11}$$

and

$$J = \frac{\nu \epsilon_s}{9L^2} (\frac{2q}{m^\star})^{1/2}. \tag{3.12}$$

Equation (3.12) is knows as Child-Langmuir law.

3.2 Poole-Frankel effect

The current-voltage characteristics of a device varies according to the strength of the applied voltage across the electrodes. At low applied voltage some charge carriers might be confined in kind of trap centres that could be characterized by electrostatic potential. Those charge carriers in trap centres could not contribute to the total current in the device. By increasing the applied external electric field (voltage) the charges might be released from

the traps and contribute to the total current. Poole and Frankel proposed a model that can take into account the contribution of charges from traps to the total current. The essence of Poole-Frankel model is that in the presence of a strong electric field the effective depth of a trap would be reduced (see figure 3.2) which facilitates the release of charge carriers from traps and contribute to the total current [17]. If we consider an electron traps as a positively charged centre at a fixed position in a structure-less dielectric, the potential energy of the electron is given by:

$$V(\mathbf{r}) = \frac{-e^2}{4\pi\epsilon\epsilon_0 r} - eEr \tag{3.13}$$

where the field E is applied in x direction. If E = 0, then the maximum value of $V(\mathbf{r}) = 0$ and occurs at infinite distance from traps. In the presence of

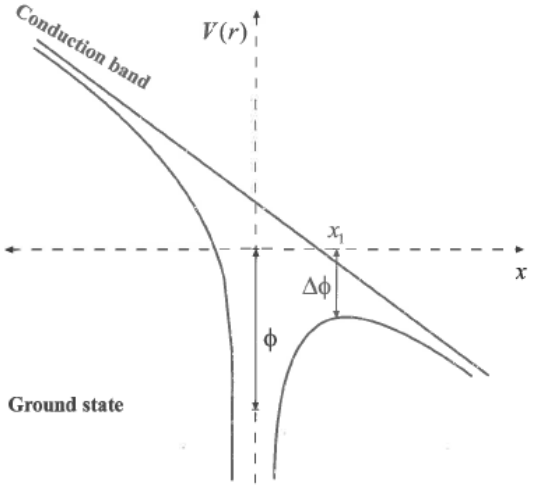

Figure 3.2: Frankel effect showing the reduction of the trap depth by $\Delta\phi$.

the applied field the maximum potential of the trap occurs at x_1 which can

be determined from equation (3.13) by the condition $\frac{dV(r)}{dx} = 0$ to give

$$x_1 = (\frac{e}{4\pi\epsilon\epsilon_0 E})^{1/2}. \tag{3.14}$$

The value of the potential at x_1 (which is the same as $\Delta\phi$) becomes:

$$\Delta\phi = -(\frac{e^3 E}{\pi\epsilon\epsilon_0})^{1/2}. \tag{3.15}$$

By considering a single trap level with energy ϕ beneath the conduction band, the ratio of free charge carrier density (ρ_f) and the density of traps (ρ_t) can be written as

$$\begin{aligned} \frac{\rho_f}{\rho_f + \rho_t} &= \frac{N_c}{N_t} exp[-\frac{\phi}{kT} + \frac{1}{kT}(\frac{e^3 E}{\pi\epsilon\epsilon_0})^{1/2}] \\ &= \Theta_0 exp(\gamma E^{1/2}) \end{aligned} \tag{3.16}$$

where $\gamma = \frac{1}{kT}(\frac{e^3}{\pi\epsilon\epsilon_0})^{1/2}$. Note that N_c and N_t are the effective density of states in the conduction band and the density of traps respectively. The Frankel effect is likely to have observable consequences if $\gamma E^{1/2}$ is of order unity or greater. With the aid of numerical integration the current density is then modified as;

$$J = \frac{8}{9}\mu\epsilon\epsilon_0 \frac{V^2}{L^3} e^{[\frac{0.891}{kT}(\frac{e^3 V}{\pi\epsilon\epsilon_0 L})^{1/2}]}. \tag{3.17}$$

Equation (3.17) represents the current density across two electrodes in the presence of traps and Frankel effect in the medium. Note that the electric field is assumed to be uniform in the conductor and is given by $\overrightarrow{E} = V/L$.

3.3 Conducting Polymers

Conducting polymers are organic compounds (often called organic semiconductors or conjugated polymers) which have tremendous application potential in the areas of electronic, optoelectronic, and sensory applications. They have emerged as a basic and cheap materials in the fabrication of devices such as light emitting diodes, thin film transistors, photovoltaic cells, and plastic lasers, to name a few. Conjugated polymers are polyunsaturated compounds whose backbone atoms are sp- or sp^2- hybridised. Conjugated polymers, in their pristine, neutral state-, are either insulators or wide-gap semiconductors, and some of them turn into metallic type conductors only after a process called **doping**. Doping here is the process of adding or removing electrons from the polymer chain. There are several ways of doping conjugated polymers such as Chemical doping by charge transfer, Electrochemical doping and Photo-doping.

Chemical doping: is the most frequently used method of doping conjugated polymers which can be accomplished by the process called oxidation or reduction via the interaction of the polymer with either the oxidising or reducing agent. **Electrochemical doping:** is another way of doping technique which can be carried out by applying external electric potential on the electrodes immersed in a solution containing the conjugated polymer. **Photo-doping:** is the process of removing (adding) electrons from the polymer chain by exposing them to intense electromagnetic radiation.

The mechanism by which the polymers conduct electricity has been the source of controversy ever since conducting polymers were first discovered. Unlike metals where the electron gas is thought to be responsible for electrical conduction, the charge transport in conjugated polymers occurs via the involvement quasi-particles such as excitons, polarons, and bi-polarons. These quasi-particles are often created during the doping process which enhances the electrical conduction of the pristine polymer. In metals, conductivity increases with decreasing temperature the lattice vibrations freeze out. However, in conducting polymer conductivity decreases exponentially with decreasing temperature. This suggests that charge transport in conducting polymer is assisted by thermal energy which is different from the mechanism in metals.

3.4 Energy Band description of the conjugated polymers

The molecular orbital theory defines that when two atoms bond to form a molecule, the atomic orbitals overlap to form a molecular orbitals. Depending on the bonding energy of the molecule two possible energy levels are formed these are called bonding and anti-bonding. The electrons are allowed to occupy these molecular orbitals according to the Pauli Exclusion Principle. These molecular orbitals form energy band in the bulk of the material composed of the molecules. From Figure (3.3) the energy difference between the highest occupied molecular orbital (HOMO) and lowest unoccupied molecu-

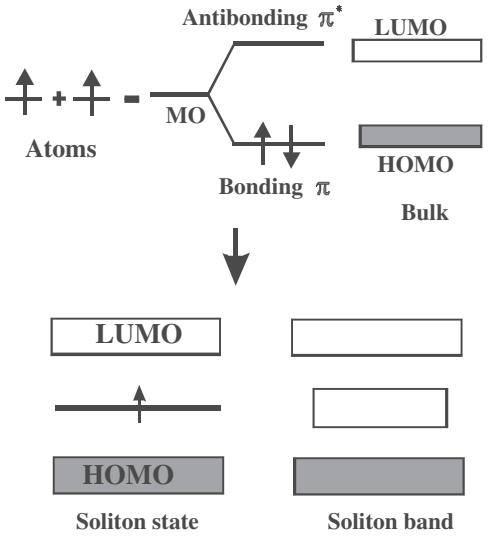

Figure 3.3: The energy band diagram of conducting polymers.

lar orbital (LUMO) is assigned as the energy bands gap of the material. The HOMO-LUMO level is analogous to the valence band and the conduction band in inorganic materials.

3.5 Solar Cell

A solar cell is a device that converts solar energy to electrical energy by harvesting the solar radiation using photo-active materials. Various materials have been employed in the fabrication of solar cells that include silicon, and gallium-arsenide. However, recently organic materials have shown promising results to be used as cheap photo-active elements of organic solar cells. The device structure of a solar cell has the form of a simple diode which is often formed at the junction of p-type and n-type semi or/and near metal semiconductor interfaces. Therefore, the important parameters that characterizes

the solar cell can be derived from a diode equation that relates the external applied voltage (V) and the amount of current from the cell at a given temperature. Generally, the current-voltage characteristics of a solar cell obeys the diode equation, however, when the cell is exposed to electromagnetic radiation excess charges will be generated by incident photons which enable the device to convert solar energy to electricity. If I_{ph} is the current generated by incident photons then the current in the solar cell can be written as:

$$I = I_s(e^{qV/kT} - 1) - I_{ph} \tag{3.18}$$

where I_s is the saturation current. The open circuit voltage is obtained when $I = 0$ in equation (3.18)

$$V_{OC} = \frac{kT}{q} ln(\frac{I_{pn}}{I_s} + 1) \approx \frac{kT}{q} ln(\frac{I_{ph}}{I_s}). \tag{3.19}$$

The short circuit current is obtained when $V = 0$ to give

$$I_{SC} = I_{ph}. \tag{3.20}$$

The power output will be

$$\begin{aligned} P &= IV \\ P &= [I_s(e^{qV/kT} - 1) - I_{ph}]V. \end{aligned} \tag{3.21}$$

The condition for maximum power is obtained when $\frac{dP}{dV} = 0$

$$\begin{aligned} V_m &= \frac{kT}{q} ln(\frac{1 + (I_{ph}/I_s)}{1 + (qV_m/kT)}) \\ I_m &= I_s(\frac{qV_m}{kT}) e^{qV_m/kT}. \end{aligned}$$

Finally, the power conversion efficiency of a solar cell is determined by the relation given by:

$$\begin{aligned} \eta &= \frac{I_m V_m}{P_{in}} \\ &= \frac{(FF) I_{SC} V_{OC}}{P_{in}} \end{aligned}$$

where the fill factor (FF) is defined by:

$$FF = \frac{I_m V_m}{I_{SC} V_{OC}}$$

In order to maximise the power conversion efficiency of the cell, we need maximise FF, I_{SC} and V_{OC}. The I-V characteristic equation defined by equation (3.18) describes the behaviour an ideal diode. The current in a real solar cell encounters resistances from contacts as well as the photo-active medium of the cell. This behaviour can be described by a simple equivalent circuit, in which a diode and a current source are connected in parallel as shown in Figure 3.4. In practice the FF is influenced by the series resistance, R_s, and the shunt resistance, R_p, of a solar cell. The influence of these parameters on the I-V characteristic of the solar cell can be studied using the equivalent circuit presented in Figure (3.4). The I-V characteristic of the one-diode equivalent

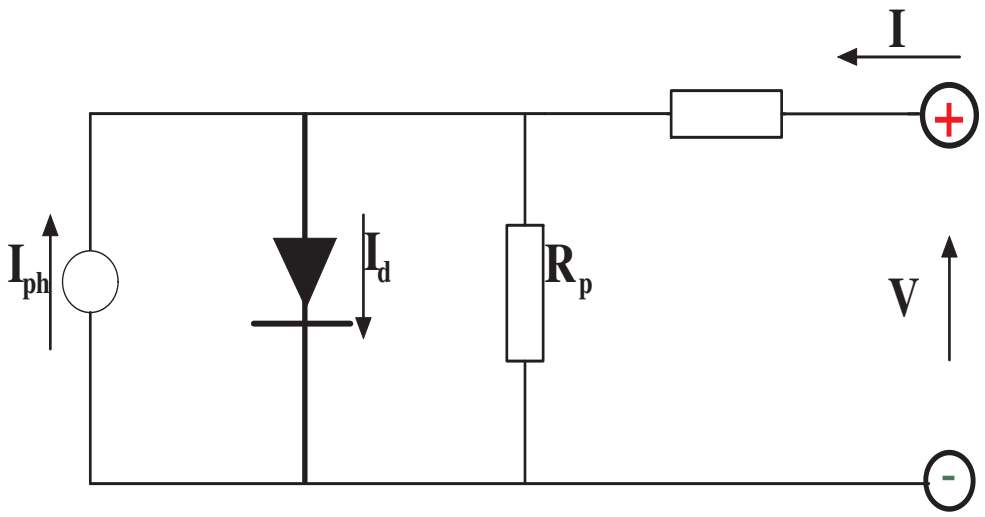

Figure 3.4: The equivalent circuit of an ideal solar cell.

circuit with the series resistance and the shunt resistance is described by:

$$I_s = [e^{\frac{q(V-IR_s)}{kT}} - 1] + \frac{V - IR_s}{R_p} - I_{ph} \tag{3.22}$$

where R_s is the series resistance, R_p is the shunt resistance, and A is the area of the cell. As the series resistance increases, the voltage drop between the junction voltage and the terminal voltage becomes greater for the same current. The result is that the current-controlled portion of the I-V curve begins to sag towards the origin, producing a significant decrease in the terminal voltage and a slight reduction in I_{SC}, the short-circuit current. High values of R_S will also produce a significant reduction in I_{SC}. In these regimes, the series resistance dominates and the behaviour of the solar cell resembles that of a resistor. As the shunt resistance decreases, the current diverted through the shunt resistor increases for a given level of junction voltage. The

result is that the voltage-controlled portion of the I-V curve begins to sag towards the origin, producing a significant decrease in the terminal current I and a slight reduction in V_{OC}. A low value of R_{SH} will produce a significant reduction in V_{OC}.

Chapter 4

Organic Photovoltaic Cells (OPV)

4.1 Introduction

The most widely used organic semiconductor device architecture is a metal-semiconductor-metal (MSM) structure using two metal electrodes with asymmetric work functions. This structure is composed of a thin layer of conducting polymer sandwiched between two metals that have different work functions. The device is built up by sequential deposition of the device elements one after the other. The metal-semiconductor-metal stack shown in Figure 4.1 uses the indium thin oxide(ITO) as a transparent electrode on glass substrate and another metal electrode on the top. LiF and PEDOT:PSS are included to improve the collection of the charges from the active medium. The working principle of organic PV cells follows few basic steps that include the absorption of electromagnetic radiation, exciton generation and

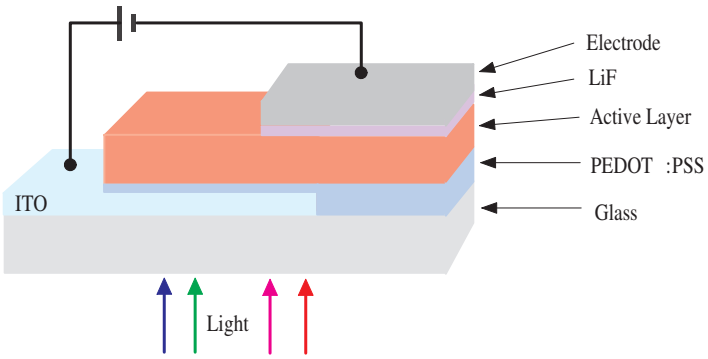

Figure 4.1: Device structure of organic photovoltaic cell.

diffusion, charge separation and charge collection. When electromagnetic radiation shines on the photo-active component of the OPV cell quasi-particles called excitons will be created in the photon-active layer of the cell. The excitons then diffuse in the medium until they encounter an electrostatic field which breaks them into free electron-hole pairs. The free charge carriers are driven by the field towards the electrodes and finally collected as an electric current. The effectiveness of a photovoltaic device depends upon the nature of the photo-active layer and the methods used to collect the charges and to the external circuit.

4.1.1 Light Absorption

In most organic devices only a small portion of the incident light is absorbed because the band gap is too high. A band gap of 1.1 eV is required to absorb 77% of the solar radiation on earth whereas the majority of semiconducting polymers have band gaps higher than 2.0 eV, limiting the possible absorption to about 30% [20]. For an efficient collection of photons, the ab-

sorption spectrum of the photo-active organic layer should match the solar spectrum and the layer should be sufficiently thick to absorb most of incident light. The optical absorption coefficient(α) of organic materials is much higher than that of crystalline silicon. For conjugated polymers MDMO-PPV(polyphenylene vinylene), P3HT(Poly(3-hexylthiophene-2,5-diyl)) and for the molecular dye, zinc phthalocyanine (ZnPc) α exceeds $1 \times 10^5 \text{cm}^{-1}$[18] in the major part of the visible spectrum. The absorption coefficient spectra of MDMO-PPV and P3HT lack absorption in red and NIR (near-infrared) part of the spectrum. A photovoltaic cell based on single light absorption medium, a band-gap of approximately 1.1 eV [20] is optimal. By lowering the band gap of the polymer more photo-current can be generated. However, increasing the layer thickness is often advantageous for light absorption, but charge transportation might be impeded.

4.1.2 Exciton Diffusion

All photo-excited excitons should reach a dissociation site. Since such a site may be at the other end of the semiconductor, their diffusion length should be at least equal to the thickness of the sample (for sufficient absorption), otherwise they recombine and photons are wasted. Exciton diffusion ranges in polymers and pigments are usually around 10 nm [20]. For the realisation of an efficient organic solar cell all excitons formed due to light absorption should lead to the formation of free charge carriers. The exponential lifetime of an exciton (τ_{exc})is determined by the reciprocal value of all radiate and non-radiactive decay rates together. For an efficient solar cell, excitons have

to reach the photo-active interface within the time τ_{exc}. Transport of the exciton occurs by diffusion and the distance an exciton is able to cross, L_{exc}, is given by:

$$L_{exc} = \sqrt{D_{exc}\tau_{exc}} \tag{4.1}$$

in which D_{exc} is the diffusion coefficient of the exciton. Since for molecular materials τ_{exc} is often only several nanoseconds at most, L_{exc} is generally limited to 10 nm [22]. In practice this implies that only those exciton formed within a distance of L_{exc} from the interface will contribute to charge separation.

4.1.3 Charge separation

Creation of charges is one of the key steps in the conversion of solar light into electrical energy. In most organic solar cells, charges are created by photo-induced electron transfer [10]. In this process an electron is transferred from an electron donor (D) material to an electron acceptor (A) material with the aid of the additional input energy of an absorbed photon with energy $h\nu$ [10]. An electron donor is characterized by a molecular material with a small electron affinity. Vice versa an electron acceptor is a material with a high electron affinity. The difference between both electron affinity levels is the driving force required for the exciton dissociation. In the photo-induced electron transfer process an exciton at the D/A interface decays by creation of the charge-separated state consisting of the radical cation of the donor(D^+)

and the radical anion of the acceptor(A^-) as follows.

$$D + A + h\nu \rightarrow D^* + A (or D + A^*) \rightarrow D^{\bullet +} + A^{\bullet -} \tag{4.2}$$

For an efficient charge generation, it is essential that the charge-separated state is the thermodynamically and kinetically most favourable pathway for the exciton [20]. Therefore, it is important that the energy of the absorbed photon is used for generation of the charge separated state and is not lost via competitive processes like fluorescence or non-radioactive decay [22]. In addition, the charge-separated state should be stabilised, so that the photo-generated charges can migrate to one of the electrodes. Therefore, the back electron transfer or recombination should be slowed down as much as possible [20].

4.1.4 Charge collection

In order to enter an electrode material with a relatively low work-function(Al or Ca) the charges often have to overcome the potential barrier of thin oxide layer. The metal may have formed a blocking contact with the semiconductor so that they cannot immediately reach the metal. The collection of charge carriers at the electrodes is regularly accomplished by a transparent conductive oxide (TCO) such as ITO or SnO_2:F on one side and a metal contact on the other side. Ohmic contact between the electrodes and the molecular layers is then formed. In practice special contact layers have been developed to obtain better performance of the solar cell. Examples of contact layers are a PEDOT:PSS (poly(3,4-ethylenedioxythiophene)

poly(styrenesulfonate)) layer, which is a charged conducting polymer layer at the TCO side and LiF layers at the metal contact [22].

4.2 Device Structures

4.2.1 Single layer cells

The first organic solar cells were based on single thermally evaporated molecular organic layers sandwiched between two metal electrodes of different work functions. The rectifying behaviour of these devices can be explained by the MIM-model (for insulators) or by the formation of a Schottky barrier (for doped materials) between the metal with the lower work function and the p-type organic layer [21].

This cell consists of only one semiconductor material and is often referred to as a Schottky type device or Schottky diode since charge separation occurs at the rectifying (Schottky) junction with one electrode. The other electrode interface is supposed to be Ohmic in nature [26]. The structure is simple but an absorption covering the entire visible range is rare using a single type of molecule. The photo-active region is often very thin and since both positive and negative photo-excited charges may travel through the same material recombination losses are generally high. Such cells are currently used for screening and evaluation purposes [26].

4.2.2 Double layer cells

In an attempt to improve the performance of organic molecule based solar cells, another device structure was designed by making layers of p-type and n-type polymers sandwiched between two electrodes. For this cell configuration of the photo-generated excitons in the photo-active material have to reach the p-n interface where charge transfer can occur [22], before the excitation energy of the exciton is lost via intrinsic radiate and non-radiactive decay rates processes to the ground state. Because the short exciton diffusion length of the organic material, which is in general limited to $5 - 10$ nm, only absorption of light within a very thin region around the interface contributes to the photovoltaic effect. This limits the performance of double-layer devices, because such thin layers cannot absorb all the incident light [10, 20].

A strategy to improve the efficiency of the double-layer cell is related to structural organisation of the organic material to extend the exciton diffusion length and, therefore, create a thicker photo-active inter-facial area [22, 26]. Double layer cells benefit from separated charge transport layers that ensure connectivity with the correct electrode and give a separated charge carrier only a small chance to recombine with its counterpart. The drawback is the small interface thickness that allows only excitons of a thin layer (exciton diffusion length + depletion layer thickness) to reach it and become dissociated [26].

4.2.3 Bulk Heterojunction cells

The bulk heterojunction (BHJ) design is based on the mixture of both p-type and n-type polymers which create molecular interfacial layers that enhance the separation of excitons into free charge carriers. Due to the short lifetime, and low mobility and short diffusion length of excitons in organic semiconductors. There was a need to find a mechanism to dissociate excitons before losing them by recombination. The advantages of BHJ is that excitons can be dissociated anywhere in the active layer where there exists p-and-n type molecular interfaces. The distance to the interfaces should be of the order of the exciton diffusion length. Despite their high absorption coefficients, exceeding 1×10^5 cm^{-1}, a 20 nm double layer of donor and acceptor materials would not be optical dense, allowing most photons to pass freely [20]. The solution to this dilemma is elegantly simple, by mixing the p-and n-type materials, junctions throughout the bulk of the material are created that ensure each photo-generated exciton leads to charge transfer, irrespective of the thickness of the layer [20]. Mixtures, based on substituted fullerenes (with acronym PCBM) and DMOM-PPV were among the first materials to utilize this bulk-hetero- junction principle [22].

Photo-generated charges must be able to migrate to the collecting electrodes through this composite material. Because holes are transported by the p-type semiconductor and electrons by the n-type material, these materials should be preferably mixed into a bi-continuous, inter-penetrating network [20]. In Figure 4.2 a bulk heterojunction schematically shown. The bulk heterojunc-

tion is presently the most widely used photo-active layer for realisation of organic solar cells.

The name bulk-heterojunction solar cell has been chosen, because the interface between two different components (heterojunction) is all over the bulk, in contrast to the classical (bi-layer) junction [20]. Control of morphology is not only required for a large charge-generating interface and suppression of exciton loss, but also to ensure percolation pathways for both electron and hole transport to the collecting electrodes [20].

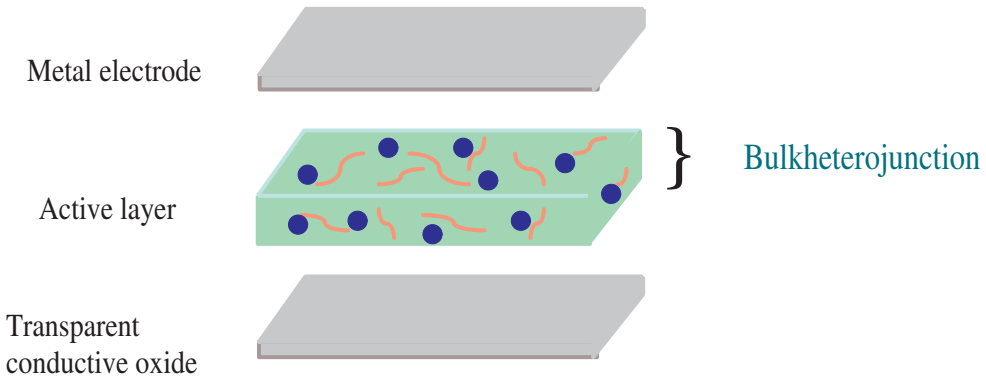

Figure 4.2: Schematic view of the bulkheterojunction active layer where p- and n-type polymers are blended to enhance donor-acceptor interfaces.

The electrical current densities are mainly limited by incomplete utilisation of the incident light due to a poor match of the absorption spectrum of the active layer with the solar spectrum, and low charge carrier mobility of the organic or polymer semiconductors. In this respect, the use of P3HT, which is known to have a high charge-carrier mobility and reduced band-

gap compared to MDMO-PPV, has been considered for use in solar cells in combination with PCBM [10, 20]. P3HT/PCBM blends indeed exhibit an increased performance compared to MDMO-PPV. The higher efficiency was obtained through the use of post-production treatment. After spin coating of the active layer and deposition of the aluminium top electrode, treating P3HT/PCBM solar cells by applying a voltage higher than the open circuit voltage and a temperature higher than the glass transition temperature of approximately 120°C led to an improved overall efficiency [20]. This post-production treatment enhances the crystallinity of the P3HT and improves the charge carrier mobility. Photovoltaic devices of P3HT/PCBM have reached power conversion efficiency of close to 5% [26].

4.2.4 Charge carrier transport models in BHJ

The performance of an organic photovoltaic cell depends critically on the mobility of charge carriers within the constituent organic molecules. Because of the disordered nature of the polymer medium no single model, so far, was able to describe the conductivity of the polymers for all ranges of doping level and temperature. However, a complex combination of phenomena that span a range of length and time scales control charge transport in disordered organic semiconductors. As a result, it is difficult to rationalise charge transport properties in terms of material parameters.

Hopping transport mechanism is among the few successful models that was often used to describe the transport phenomena in disordered system. The

mobility of electrons in organic molecules is relatively small (< 0.1 cm^2/Vs) compared to inorganic semiconductors (100 - 10000 cm^2/Vs) [20]. Bassler[27] proposed a hopping transport model as a mechanism for charge transport in disordered organic systems. He further assumed that the hopping rates can be described by the Miller-Abraham's formalism[42] where the charges hop in a regular array of hopping sites. In this way both positional disorder and energetic disorder are introduced (See Figure 4.3). In this model, the energy distribution of localised states can be approximated by a Gaussian function [27]:

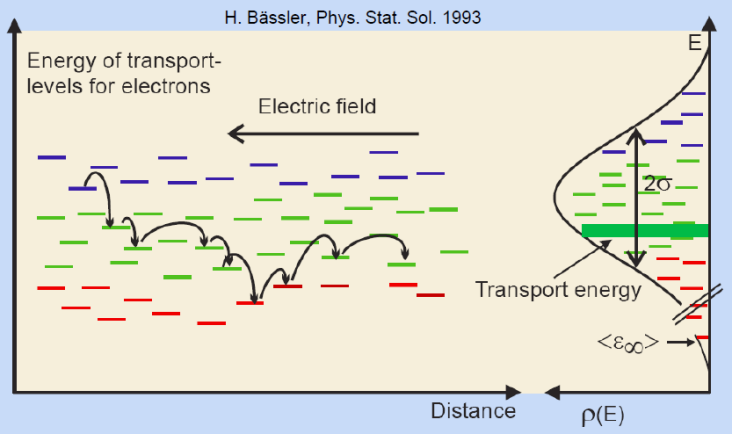

Figure 4.3: Energetic and spatial disordered system of polymer medium [27].

$$\rho(\varepsilon) = \frac{1}{\sqrt{2\pi\sigma^2}} \times exp(-\frac{\varepsilon^2}{2\sigma^2})$$

The energy is measured relative to the centre of the DOS. The jump rate among sites i and j is assumed to be Miller-Abraham's type; given by

$$\nu_{i\to j} \;=\; \nu_0 exp(-2\gamma\Delta R_{ij}) \times exp(-\frac{E_j - E_i}{kT}) \tag{4.3}$$

if $E_j > E_i$, where ν_0 hopping frequency "attempt to escape frequency", γ is overlap parameter. E_i and R_{ij} represent energetic and positional disorder [25]. On the basis of the Monte Carlo simulations, the charge carrier mobility is temperature-and field-dependent, and in the limit of high electric fields is given by [27]:

$$\mu(E,T) \;=\; \mu_0 exp[-(\frac{3\sigma}{5kT})^2] \times exp[C(\frac{\sigma}{kT})^2 - \Sigma^2)\sqrt{E}] \tag{4.4}$$

for $\Sigma \geq 1.5$.

Chapter 5

Experimental

5.1 I-V Characteristics of a diode

The largest amount of emission of radiation from the sun occurs in the visible and infrared regions of the solar spectrum. In order to harvest a significant portion of the radiation using photovoltaic cells we need to prepare the photo-active layer from low energy band gap materials (0.5-2.0) eV. The low band gap conducting polymers are among few materials that can be used for large scale photovoltaic devices.

Current-Voltage characteristics of the photovoltaic cell diodes taken from a test solar cell under dark and illumination conditions is given in Figure (5.1). In Figure (5.1), Under the dark conditions the current from the cell is too low or none for both reverse and forward voltages. As the external voltage increases beyond the open circuit voltage, then the current will be injected from the electrodes and the current increases. However, when the device is

exposed to white light, the current will be generated causing the curve to be lifted up even in the absence of external voltage (V = 0). The current under illumination measured in the absence of external voltage ($V = 0$) is called short circuit current (I_{SC}). Similarly, the open circuit voltage (V_{OC}) is defined as the potential that develops across the terminal of the solar cell in the absence of current in the circuit ($J = 0$). Maximum power (P_{max}) is

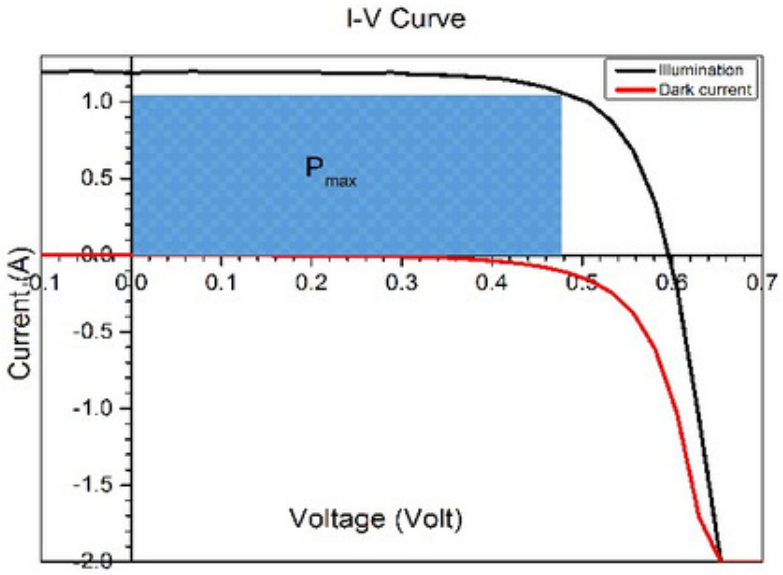

Figure 5.1: Current-Voltage curve in dark and under illumination.

determined by the largest rectangle drawn in the first quadrant of the I-V curve as depicted in the Figure (5.1). The parameters that characterizes the solar cell are fill factor (FF), open circuit voltage (V_{OC}) and short circuit current (I_{SC}). The fill factor is defined as the ratio of the maximum power

(P_{max}) to the area of the rectangle formed by V_{OC} and I_{SC} hence

$$FF = \frac{V_{max} I_{max}}{V_{OC} I_{SC}}. \tag{5.1}$$

The efficiency of a solar cell is the ratio of electrical power that gets delivered to the load of the optical power in the cell. Maximum efficiency is achieved when the power delivered to the load is the maximum power. Incident optical power is normally specified as the solar power on the surface of the earth which is approximately 100 mW/cm^2. The efficiency of the cell is given as follows:

$$\eta = \frac{P_{max}}{P_{in}} = \frac{(V_{OC})(I_{SC})(FF)}{P_{in}}. \tag{5.2}$$

When a solar cell is working, the current decreases and a voltage develops as charge builds up at the terminals. The resulting current can be viewed as a superposition of the short circuit current, caused by the absorption of photons, and a dark current, which is caused by the potential built up over the load and flows in the opposite direction [28]. When a solar cell is formed from a pn-junction, it may be treated as a diode. For an ideal diode, the dark current density equation is given by [29]:

$$J_{dark}(V) = J_0(e^{qV/k_B T} - 1) \tag{5.3}$$

where J_0 is a constant called *saturation current*, q is the electron charge and V is the voltage between the terminals. The resulting current can be approximated as a superposition of the short circuit current and the dark

current[29]:

$$J = J_{SC} - J_0(e^{qV/k_BT} - 1). \tag{5.4}$$

To find an expression for the open circuit voltage (V_{OC}), one needs to impose the condition J=0 to equation (5.4) [29]. This means that the two currents cancel out so that no current flows, which is exactly what is expected in the case of an open circuit voltage ($V = V_{OC}$). Thus, the resulting expression is [29]:

$$V_{OC} = \frac{k_BT}{q} ln(\frac{J_{SC}}{J_0} + 1) \tag{5.5}$$

where J_{SC} is directly proportional to the incident optical power (P_{in}). The open circuit voltage of the solar cell is expected to increase logarithmically with incident power. The saturation current J_0 can be obtained from the measured dark current.

For device characteristics we follow the steps below:

- The device characteristics are studied using I-V measurements under dark and illumination conditions.
- One needs to determine(V_{OC})and (I_{SC}) of the diode,
- and to calculate important parameters such as fill factor (FF, given by equation 5.1) and efficiency (given by equation 5.2) of the cell.

5.2 Device Preparation

An ITO-coated glass was used as a substrate for the preparation of the samples. The first step in device preparation is to remove part of the ITO from the surface of the glass substrate. This can be done by protecting half of the ITO-coated glass with photo-resist tape, and followed by etching the unprotected ITO-coated glass inside warm acid solution. The acid solution was prepared with the concentration of 48% of HCl, 48% of H_2O, and 4% of HN_3O.

The samples were then cleaned firstly by rinsing the sample in the running tap water. Followed by cleaning using labcon model L1BM80 Ultrasonic Cleaner with detergent and distilled water. Thereafter, the samples were ultra-sonicated using acetone, and isopropanol subsequently for 10 minutes holding time. Then the substrate was left to dry inside the oven at about 50°C.

The photo-active layer of the devices were prepared from the mixture of P3HT and PCBM polymers in the chloroform solvent. The P3HT and PCBM are blended at stoichiometric ratio 1:1 and 1:0.8 by weight. The concentration of the solution used was 20 mg/ml.

Spin coating is a precise and very simple method to produce a uniform thin film ranging from 20 to 300 nm thickness. One can easily change the spin speed and the concentration of the solution so that we can control the uni-

formity of the layer. The photo-active layer of organic photovoltaic cells have thickness ranging from 100 to 200 nm. During spin-casting, volatile chloroform solvent is evaporated and spin time is typically between 30 to 60 seconds (Figure 5.2). Hole conducting polymer PEDOT:PSS was first spin

Figure 5.2: PI-KEM LTD Spin Coater KW-4A.

coated on cleaned ITO coated glass substrate at the rate of 3000 RPM for 50 seconds (using the spin coater in Figure 5.2). The PEDOT:PSS was partially removed from the glass side of the substrate using water rinsed "cotton ball". The sample was then be dried in an oven at 120°C for 5 min before coating the photo-active layer. Finally, the solution composed of P3HT/PCBM was spun coated at the rate of 1300 RPM. The devices were then taken into an Edward Auto 306 vacuum evaporation chamber (Figure 5.3) where the LiF(0.6 nm) and Al(60 nm) were respectively deposited on the active layer of the device. The depositions were carried out in a vacuum as low as $\sim 10^{-6}$ mbar . At last, the devices at this stage were ready for characterization. The I-V data was taken using a Keithly 2400 source meter interfaced to computer.

Figure 5.3: Auto 306 Vacuum Coater.

Chapter 6

Results and Discussion

6.1 Optical Properties

The optical absorption properties of the polymers used were studied using UV-VIS spectroscopy. Figure 6.1 shows the absorption of P3HT in visible range of the energy spectrum. This polymer absorbs electromagnetic radiation mainly in the range of wavelengths from 350 nm to 600 nm. From the onset of the absorption it is possible to determine the band gap of the polymers. The energy band gaps of the polymers (P3HT, PEDOT:PSS, and PCBM) were determined from the onset of absorption peak. That is by measuring the wavelength(λ) corresponding to the start of absorption (Figure 6.1, 6.2 and 6.3).

The PEDOT:PSS is almost transparent to the radiation for wavelengths from 300 nm to 900 nm depicted in Figure 6.2. Furthermore, the polymer which plays as an acceptor in our investigation is PCBM. Figure 6.3 shows the op-

tical absorption spectrum of PCBM in the wavelength range from 250 nm to 700 nm. As depicted in the diagram the onset of the absorption starts from nearly 700 nm but weak intensities. However, the intensity of the absorption increases for higher energy of photons (lower wavelength). Maximum absorption intensity is observed around 450 nm.

Energy band-gap for P3HT, PEDOT:PSS and PCBM can be calculated using the following equation

$$E_g = h\nu = \frac{hc}{\lambda} \tag{6.1}$$

where $h = 6.6260688 \times 10^{-34}$ J.s is called Planck's constant, $c = 2.99792458 \times 10^8$ m/s is speed of light.

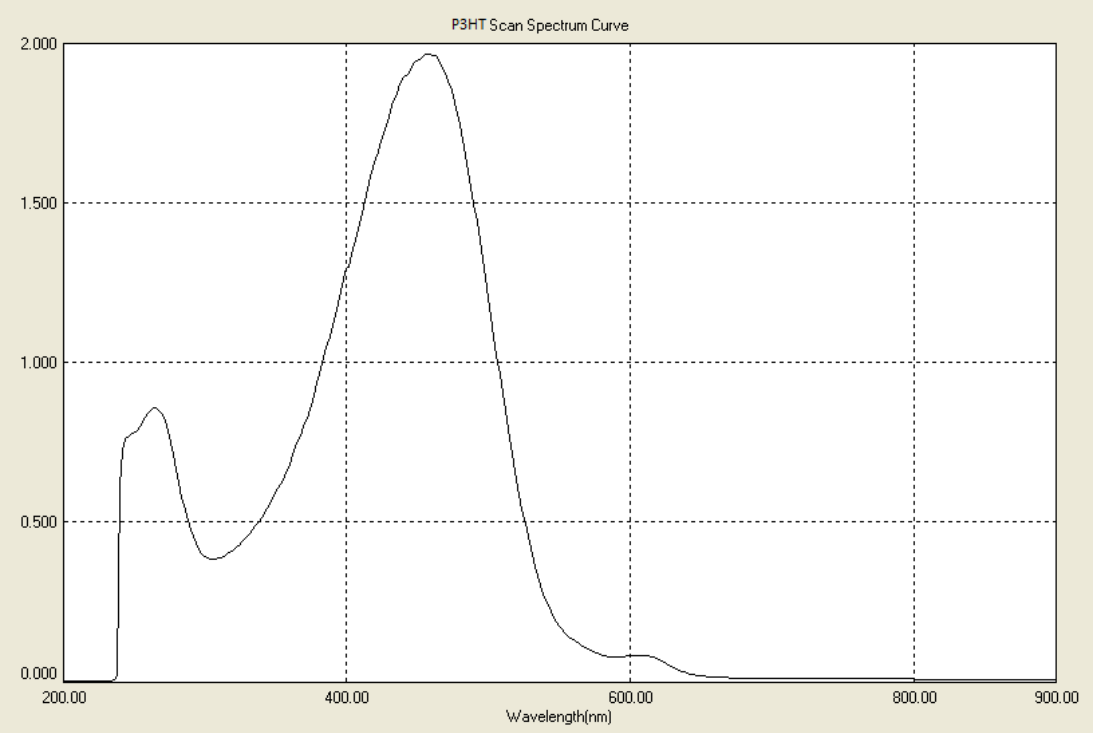

Figure 6.1: Optical absorption spectrum of P3HT.

P3HT: $\lambda = 581$ nm from Figure 6.1,

$$\begin{aligned} E_g &= \frac{1.986 \times 10^{-25}}{581 \times 10^{-9}} \\ &= 3.418 \times 10^{-19} J \\ &\approx 2.1 eV. \end{aligned}$$

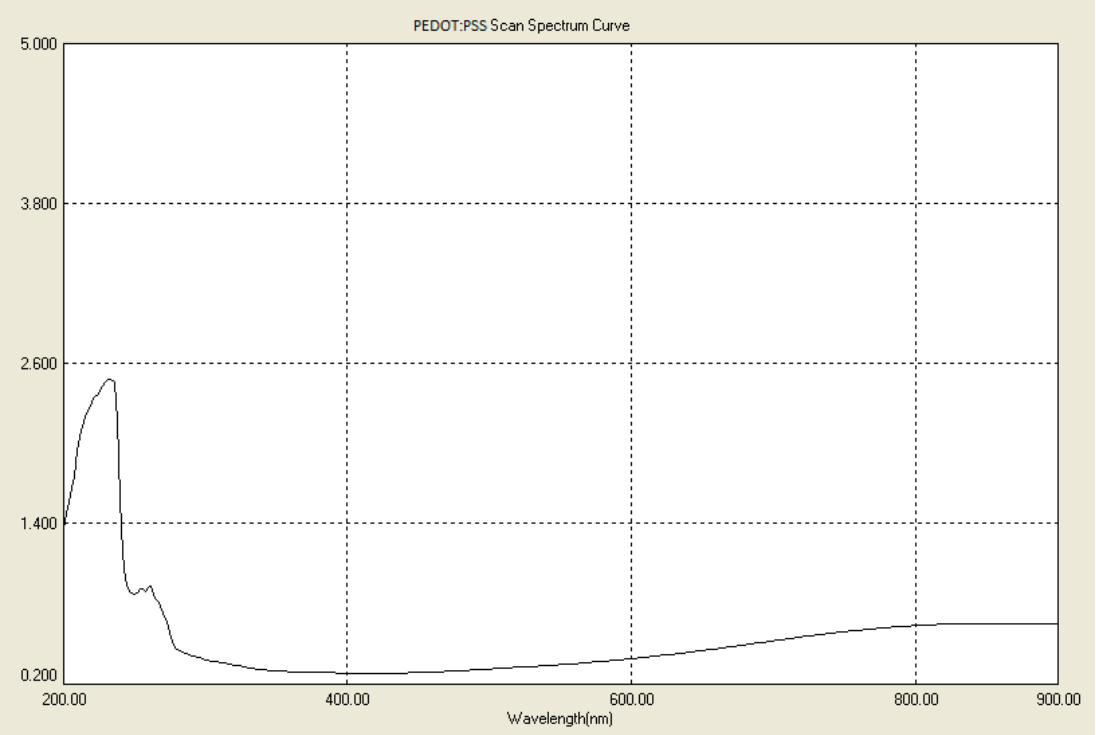

Figure 6.2: Optical absorption spectrum of PEDOT:PSS.

PEDOT:PSS: $\lambda = 343$ nm from Figure 6.2,

$$\begin{aligned} E_g &= \frac{1.986 \times 10^{-25}}{343 \times 10^{-9}} \\ &= 5.790 \times 10^{-19} J \\ &\approx 3.6 eV. \end{aligned}$$

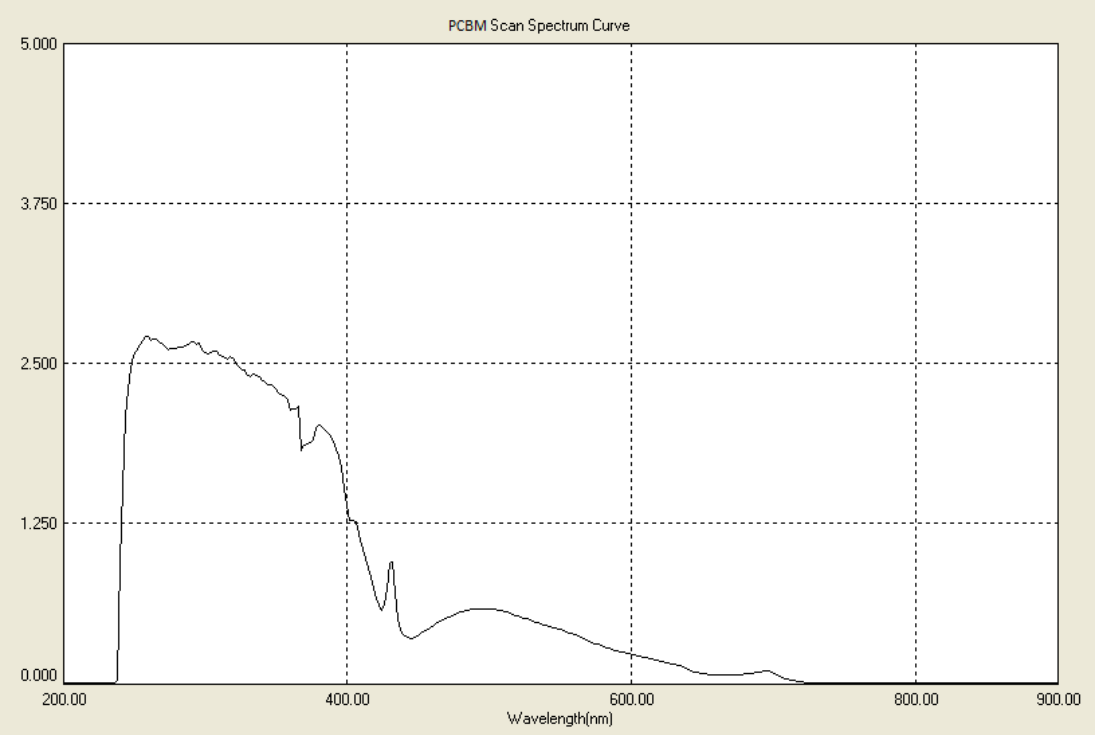

Figure 6.3: Optical absorption spectrum of PCBM (acceptor polymer).

PCBM: $\lambda = 648$ nm and 443 nm from Figure 6.3. To calculate the energy gap we are going to use 443 nm since that is where most absorption takes place. At 645 nm a slight absorption is recorded due to complexity of chemical compounds,

$$\begin{aligned} E_g &= \frac{1.986 \times 10^{-25}}{443 \times 10^{-9}} \\ &= 4.483 \times 10^{-19} J \\ &\approx 2.8 eV. \end{aligned}$$

6.2 The Electrical Properties of P3HT/PCBM bulkheterojunction PV cell

Several bulkheterojunction photovoltaic cells were prepared using P3HT/PCBM the photo-active layer in a sandwich type device structure (see Figure 6.4). The PV cells have a sandwich type device structure where PEDOT:PSS and the photo-active layer (P3HT/PCBM) were sequentially spin coated from the solution, and followed by the deposition of LiF and Al respectively. The electrical properties of the devices produced in the laboratory were studied using a Keithly 2400 source meter and standard SS50AAA solar simulator. The data were collected both under dark and illumination conditions. The samples were scanned from -1 V to 0.8 V under illumination conditions and 1.0 Sun while we took scanning from -3.0 V to 3.0 V under dark conditions.

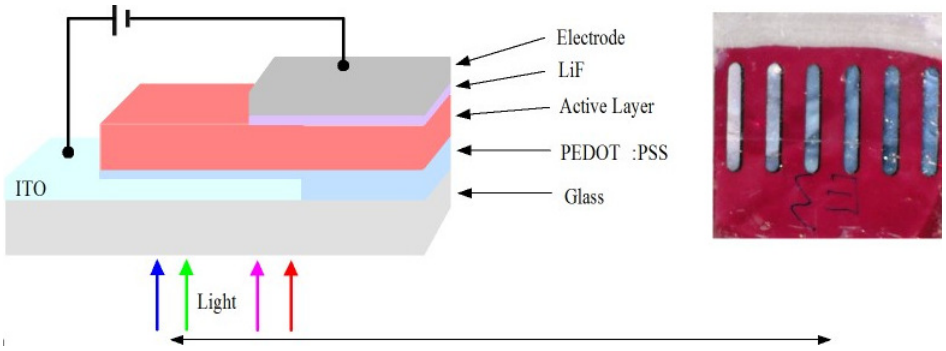

Figure 6.4: Bulkheterojunction photovoltaic cells. (a) the Schematic diagram of BHJ (b) Real BHJ solar cell produced in the lab.

Figure 6.5 shows the current voltage characteristics of one of the devices produced in this experiment. The graph carries both the dark and illumination current from the device. The current taken under illumination shows the effect of the photo-generated current at zero bias voltage as expected from prediction (equation 5.4). The short circuit current and the open circuit voltage derived from the data are 3.5 mA/cm^2 and V_{oc}=0.56, Volt respectively. However, the current under the dark condition shows almost negligible amounts of currents for all reverse voltage up until 0.4 V forward applied voltage. This is a typical property of good photovoltaic cell diodes. Figure 6.6 represents current-voltage characteristics of several diodes from the best performing sample (Sample E3). The diodes are expected to respond in the same fashion but they all differ in their short circuit current. This could be due to the relative illumination exposure time of each diode during the measurements.

6.2.1 Enhanced current density by diluting the polymer solution with fresh chloroform solvent

A new experiment was carried out by changing the conditions of the polymer solution. The polymer solution was initially prepared in the same way as the previous preparation methods. After sonicating the polymer solution for nearly 3 hours the solution was diluted with fresh chloroform solvent before coating on the sample substrate. According to the measured current-voltage characteristics from this set of devices, we found significant change in the cell parameters which suggests better performance of the PV cell.

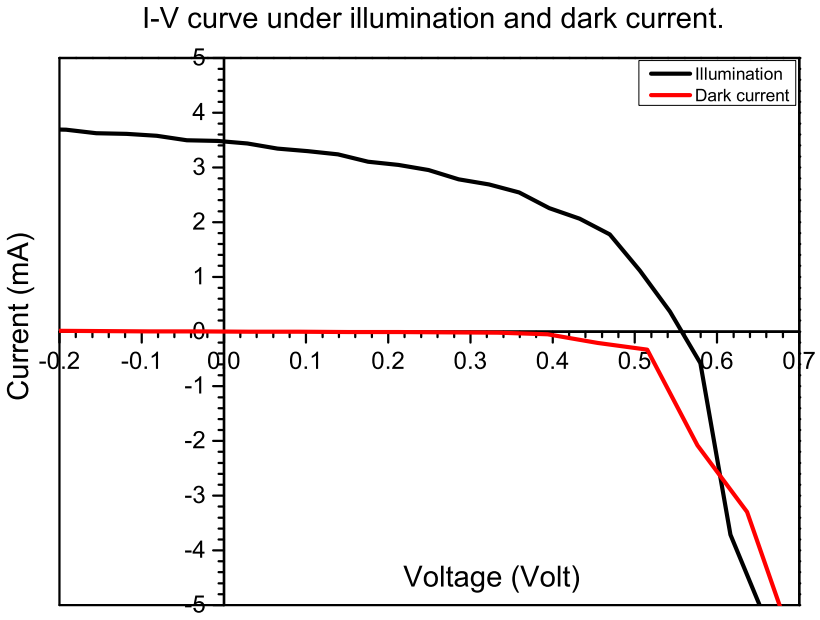

Figure 6.5: I-V curves of one of the good performing diodes both under dark and illumination conditions (sample E3).

For instance, the short circuit current (J_{SC}) of the order of 16 mA/cm^2 was recorded, which is almost four times higher than those from the undiluted solution. It was noted that for this device preparation conditions, the time taken from spin coating to placing inside the vacuum evaporation chamber was relatively shorter which reduced the polymer degradation in an open environment. Figure 6.7 shows the J-V curves taken from one of the samples prepared for investigation. From the data we were able to determine V_{OC}, J_{SC}, J_{max} and V_{max} (Figure 6.7, and Table 6.1). P_{max} was calculated by multiplying J_{max} and V_{max}. For the best sample we calculated the fill factor to be 46% and power efficiency to be 4.2%. However we had a diode that

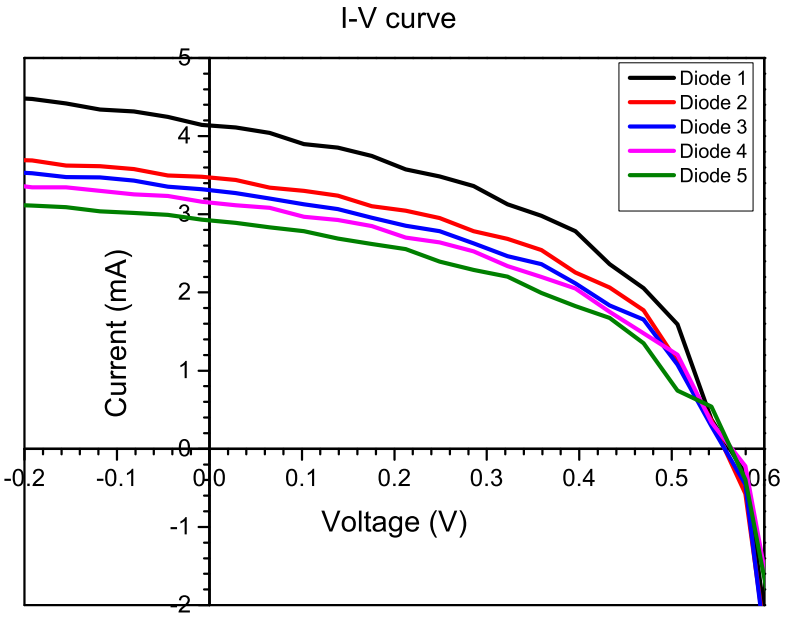

Figure 6.6: I-V characteristics for best performing sample under illumination.

produced a fill factor of 57% and power efficiency of 5.6%, which is the best diode produced under our laboratory conditions. A low I_{SC} value can result in smaller fill factor and lower V_{OC} value compared to higher I_{SC} value. The power conversion efficiency is better compared to other samples, because the polymers were spin coated at 1300 RPM. Furthermore, the cleaning techniques were improved by using ultrasonic cleaning equipment (details are provided under device preparation section).

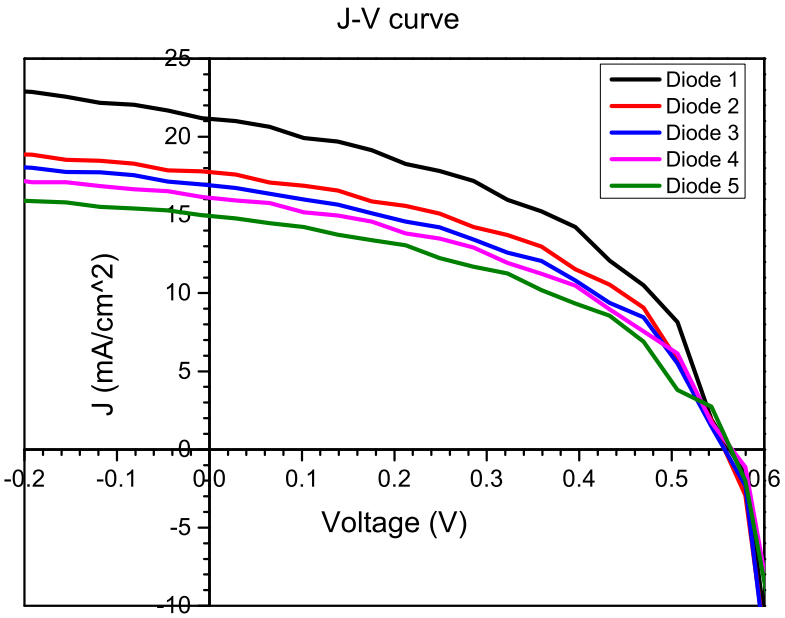

Figure 6.7: J-V characteristics for diluted polymer solution.

6.2.2 Carbon Nanotube layer between the active layers and ITO electrode

In an effort to improve the charge transport between the active layers and PEDOT:PSS we introduced a very thin layer of carbon Nanotube (CNT) with the view to enhance the performance of the devices. Nanotubes were spin coated on top of the PEDOT:PSS layer, at 4000 RPM, then warmed at 120°C in an oven.

The photo-active layer (P3HT/PCBM) was then spin coated on top the Nanotube layers followed by the deposition of LiF and Al electrodes. From

Table 6.1: Result for best sample(Sample E3 on page 71). Area=0.1757 cm^2 and Power in is equal to 0.01757 W/cm^2

Diode	V_{OC}(V)	$J_{SC}(mA/cm^2)$	FF(%)	η(%)
1	0.5627	21.2274	47	5.6
2	0.5571	17.6282	48	4.7
3	0.5571	16.8728	46	4.3
4	0.5650	16.1449	46	4.2
5	0.5641	14.9617	44	3.7

Figure (6.8), the J-V curve measured from this device shows discrepancy in the values of the open circuit voltage which could be due to the nonuniform distribution of the carbon Nanotube. In the preparation of the devices the Nanotube solution was undiluted while for P3HT/PCBM solution was diluted with chloroform solvent. In this experiment we found 2.6% power conversion efficiency from one the diodes in the sample, which is lower than the one obtained without including Nanotube (Figure 6.8). It is evident that the Nanotube solution could have washed away some of PEDOT:PSS from the substrate which affects the performance of the devices.

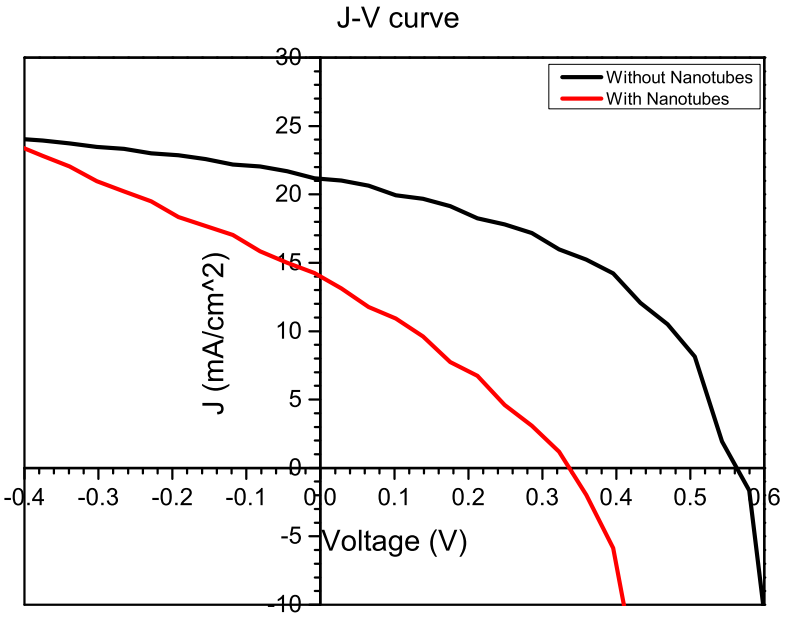

Figure 6.8: J-V curve from a sample prepared using Nanotube.

6.2.3 Charge Transport Properties

The I-V characteristics under dark conditions show typical diode knees which describes the different charge transport mechanisms of the diodes. Figure 6.9

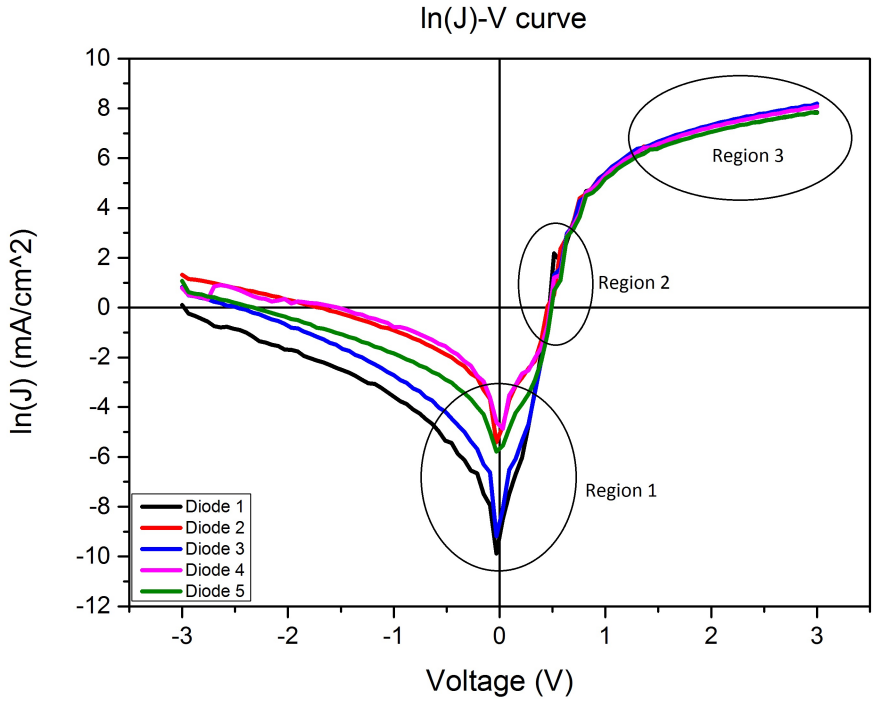

Figure 6.9: Log J versus, V graph under dark condition.

at region 1 we have a linear regime at negative voltage and low positive voltage where the current is limited mainly by shut resistance where $J \propto V$ (Ohmic contact). In region 2 there is an exponential behaviour at intermediate positive voltages where the current is controlled injection limited or, $J \propto e^{qV/kT}$ (Diffusion current). While region 3 is called a Space Charge Limited Current (SCLC) regime at high voltages where the current is limited by the shut resistance, $J \propto V^2$.

The space charge limited regime current was fitted using field dependent space charge current equation (3.8) discussed in chapter 3. From Figure (6.10) zero mobility, and field activation factor are determined (Table 6.2). The built in potential was taken from injection limited current to space charge limited regime current which in this case the amount is V_{bi}=1.4 volt. The thickness of the active layer were 180 and 200 nm. The space charge current can be described by Mott-Gurney law:

$$J = \frac{9}{8}\epsilon\epsilon_0\mu\frac{V^2}{L^3} \tag{6.2}$$

where μ is the field dependent mobility in the medium which can be written by empirical $\mu = \mu_0 e^{\gamma\sqrt{E}}$ [17]. The electric permittivity (ϵ) for polymer medium often ranges 3-5. As shown in Figure 6.10 the theoretical predictions are in a good agreement with the experimental data. From the results of the fit, important parameters such as the zero field mobility μ_0 and field activation factor γ were determined. Low mobility lead to smaller current, as expected for all organic cells. Mobility for organic photovoltaic cells can be as high as 0.1 $cm^2V^{-1}s^{-1}$ [51], and lowest can be within the range of 10^{-6} to 10^{-3} $cm^2V^{-1}s^{-1}$ [52]. The fit results (Figure 6.10) are very well in agreement with the space charge limit current theory reported in literature. We have an average mobility of 4.6×10^{-2} cm^2/V.s (Table 6.2). From the transport properties it is evident that the mobility in our devices were good [52], which contributes to the better performance of the devices.

Diode	μ_0 (cm^2/V.s)	γ ($(cm/V)^{1/2}$)	μ (cm^2/V.s)
1	0.00624	2.30×10^{-4}	$6.8{\times}10^{-3}$
2	0.0165	5.05×10^{-4}	$2.0{\times}10^{-2}$
3	0.0529	9.74×10^{-4}	$6.9{\times}10^{-2}$
4	0.0697	8.65×10^{-4}	$8.7{\times}10^{-2}$

Table 6.2: Results after fitting dark current data from best sample using SCLC.

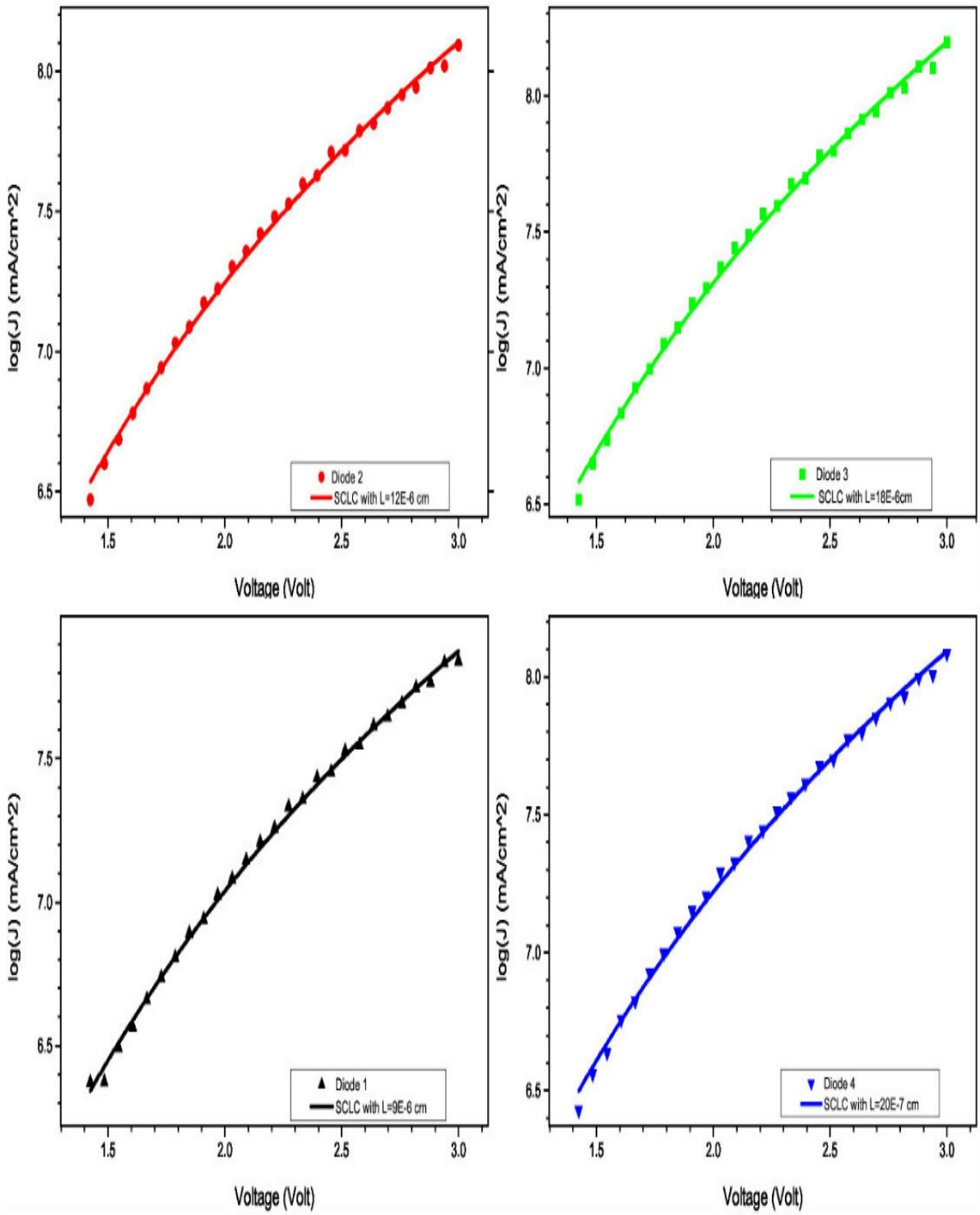

Figure 6.10: log(J) versus, V fitted with space charge limited current equation.

6.2.4 Morphology and Thickness of P3HT/PCBM

Scanning Electron Microscope (SEM) was used to study the morphology of the P3HT/PCBM photo-active layers in the devices prepared in this work. The polymers were blended at stoichiometric ratio of 1 : 0.85 and dissolved in chloroform solvent at the concentration of 20 mg/ml. Figure 6.11 was obtained for one of the best performing samples which shows a certain pattern involving the polymer chains and the distribution of PCBM in the medium. The dark zigzag lines presumably are the P3HT polymer chains while the white spots are the PCBM. The surface morphology clearly showed that there exists interpenetration network of the polymers in the photo-active medium. Such distribution of network obviously favours the creation of donor-acceptor

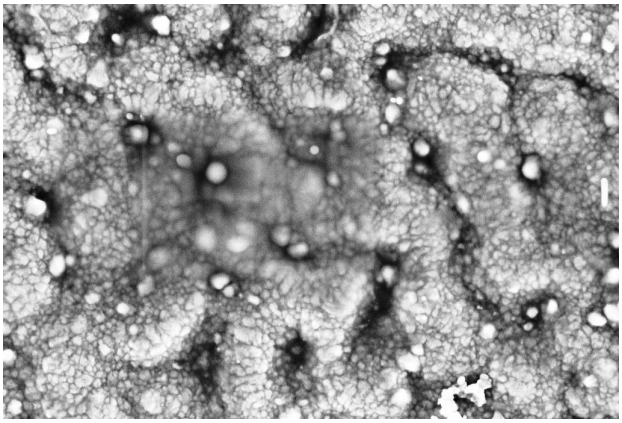

Figure 6.11: 200 nm SEM image of P3HT/PCBM BHJ active layer.

interfaces which would facilitate the dissociation of the excitons that enhances the charge transport as well as the current in the device [53]. The studies show that thicker the layer of P3HT is, the higher the chances of absorbing the light completely [54].

Chapter 7

Conclusion

In this dissertation, organic photovoltaic cells have been studied and characterized. All samples were prepared under an ambient laboratory environmental conditions. The OPV devices were of good quality and showed the typical organic photovoltaic cell properties. In an open environment of device preparation conditions, the OPV cell power conversion efficiency ranges from 1.45% up to 2.5%. However, by diluting the polymer solution with fresh chloroform solvent we found significant difference in the performance of the devices where the power conversion efficiency increases to as high as 5%. This is in fact a new development in the preparation of OPVs in simple laboratory environment.

Michael Arnold, at UW-Madison and a pioneer in developing Carbon Nanotube-based materials for solar energy applications, has proven that Nanotube solar cell can convert nearly 75% of the incident light it absorbs into electricity. It was with the intention of improving the performance of the OPV devices

that we created carbon Nanotube thin layer between the active layer and the ITO electrode. However, the results found from the experiment were not as expected. The parameters of the cell, with CNT layer, were not consistent and varied from diodes to diodes in the same sample. This could probably suggest that the Nanotubes may not be uniformly distributed on the substrate. Despite this erratic behaviour of the parameters we measured the power convection efficiency as high as 2.6% in one of the diode.

The charge transport studies suggest that the space charge limited current with field dependent mobility equation has described the measured current very well (Figure 6.10). The zero field mobility and field activation factor (Table 6.2) found in this experiment were comparable with the data available in literatures. Average field mobility measured in this experiment 4.6×10^{-2} $cm^2/V.s$ is within the expected range of the theoretical predictions [52]. One can conclude by saying that the exciton diffusion, charge separation, charge collection, and charge transport processes were successful.

Chapter 8

Outlook

More PV cells should be fabricated and tested for their stability which should be monitored over several days. In the future, a better lamp, one that is calibrated and has a spectrum that more closely matches the solar spectrum, would greatly improve the characterization process. Furthermore, glove box should be used to prepare solutions and the period it takes from preparing solution to spin coating should be minimised.

Bibliography

[1] New and Renewable Energy: Prospects in the UK for the ST Century, UK, Department of Trade and Industry, London, UK, March (1999).

[2] A.C. Mayer, S.R. Scully, B.E. Hardin, M.W. Rowell, M.D. McGehee, "Polymer-based solar cells", Stanford University, Stanford, CA 94305, USA, (2007).

[3] G. Knier, "How do Photovoltaics Work?", cited on [22 February 2013], http://www.greenpowerworks.co.za/aboutsolar.html

[4] DOE Office of Science. Basic Research Needs for Solar Energy Utilization, (2005).

[5] M. Bertolli"Solar Cell Materials", Department of Physics University of Tennes (2008).

[6] Klaus Petritsch, Organic Solar Cell Architectures, Technisch-Naturwissenschaftliche Fakultat der Technischen Universitat Graz, (2000).

[7] J.H. Schaqn, Ch. Kloc, B. Batlogg, Efficient photovoltaic energy conversion in pentacene-based heterojunctions, Appl. Phys. Lett. 77 2473 (2000).

[8] J.-M. Nunzi, C. R. Physique 3 523-542 (2002).

[9] A. Pron, P. Rannou, Laboratoire de Physique des Metaux Synthetiques, UMR 5819-SPrAM (CEA-CNRS-Univ. J. Fourier-Grenoble I), DRFMC, CEA-Grenoble, 17, rue des Martyrs, 38054 Grenoble cedex 9, France, (2001).

[10] R. Janssen, J.C. Hummelen, and N.S. Sariciftci, Polymer-Fullerene Bulk Heterojunction Solar Cells, 171040 Yulim Jung (2006).

[11] H. J. Lewerenz and H. Jungblut "Photovoltaic Grundlagen und Anwendungen" Springer, Berlin, Heidelberg, New York (1995).

[12] A.C. Arias, M. Granstrom, K. Petritsch and R.H.Friend. "Organic photodiodes using polymeric anodes" Synth. Met. 102, 953-954 (1999).

[13] A.C. Arias, K. Petritsch, M. Granstrom, J.J. Dittmer, E.A. Marseglia and R. H. Friend "Efficient Polymeric Photovoltaic Devices. " Proc. CBECIMAT (1998).

[14] W. Graupner, G. Leditzky, G. Leising, U. Scherf Phys. Rev.B 54 7610 (1996).

[15] R.I. Frank, and J. G. Simmons, J. Appl. Phys., 38, 832-40 (1967).

[16] J. R. Hook, H. E. Hall. Solid State Physics. John Wiley and Sons (2001).

[17] J. L. Frankel, Phys. Rev., 39, 4871-3(1938).

[18] J. Simon and J.J. Andre, Molecular semiconductors. Berlin-Heidelberg: Springer-Verlag.142 (1985).

[19] J. Nelson, J.J. Kwaitkowski, J. Kirkpatrick, and J.M. Frost. "*Modelling charge transport in organic photovoltaic materials*", (2009).

[20] T.J. Savenije, "Organic Solar Cells", DelftChemTech, Faculty of Applied Sciences Delft University of Technology.

[21] S.M. Sze, "Physics of Semiconductor Devices", John Wiley and Sons, New York, (1981).

[22] M. Kaushik, B. Kaushik,"Organic Solar Cells: Design, Synthesis and Characterization", International Journal of Engineering Science, ISSN 2306-64742(7) (2013).

[23] B. O'Regan and M. Gratzel, "A low-cost, high-efficiency solar cell based on dye-sensitized colloidal TiO2 films," Nature, vol. 353, no. 6346, pp. 737-740, (1991).

[24] M. K. Nazeeruddin, P. P'echy, T. Renouard, et al., "Engineering of efficient panchromatic sensitizers for nanocrystalline TiO2-based solar cells," Journal of the American Chemical Society, vol. 123, no. 8, pp. 1613-1624, (2001).

[25] W. Brtting, Charge carrier injection and transport in organic electronic devices, Institute of Physics, University of Augsburg, Germany (2007).

[26] J. Nunzi, "Organic photovoltaic materials and devices", ERT Cellules solaires photovoltaiques plastiques, Laboratoire POMA, UMR-CNRS 6136, Universit d'Angers, 2, boulevard Lavoisier, 49045 Angers, France, 2002. Hefei, Anhui 230031, (2007).

[27] H. Bassler, Phys. Stat.Sci. (1993).

[28] F. Tvora, A.S. Maia, Solar Battery charger for portable devices application, (2012).

[29] H. Lund, R. Nilsen, O. Salomatova, D. Skare, E. Riisem - (2008).

[30] M. Gratzel, "Photoelectrochemical cells," Nature, vol. 414,no. 6861, pp. 338-344, (2001).

[31] M. Gratzel, "Conversion of sunlight to electric power by nanocrystalline dye-sensitized solar cells," Journal of Photochemistry and Photobiology A, vol. 164, no. 1-3, pp. 3-14, (2004).

[32] L. Han, Y. Chiba, A. Islam, et al., "High efficiency of dyesensitized solar cells and module," in The 16th International Conference of Photochemical Conversion and Solar Storage, Uppsala, Sweden, W4-P-11 (2006).

[33] J. M. Kroon, N. J. Bakker, H. J. P. Smit, et al., "Nanocrystalline dye-sensitized solar cells having maximum performance,"Progress in Photovoltaics: Research and Applications, vol. 15, no. 1, pp. 1-18, (2007).

[34] S.Y. Dai, J. Weng, Y. Sui, et al., "Dye-sensitized solar cells,from cell to module," Solar Energy Society World Congress, vol. 84, no. 1-4, pp. 125-133, (2004).

[35] T. Yoshida, T. Oekermann, L. M. Peter, "Electrodeposition of nano-structured porous crystalline ZnO/Dye hybrid thin films for plastic solar cells, " in The 16th International Conference of Photochemical Conversion and Solar Storage, Uppsala, Sweden, , W4-O-2 (2006).

[36] C. Kittel,"Introduction to solid state physics", 7th Ed., John Wiley and Son, Inc.(1996).

[37] C. Tanase, "Unified charge transport in orderer organic",Ph.D. thesis serves (2005).

[38] E.M. Conwell, Phys. Rev. 103, 51(1956).

[39] D. Pines, Can. J. Phys. 34, 1367(1956).

[40] N.F. Mott, Can. J. Phys. 34, 1367(1956).

[41] N.F. Mott, E.A. Davis, Electronic processes in non-crystalline materials, 2nd Ed., Oxford /university Press, London (1979).

[42] A.Miller, E.Abrahams, Phys. Rev. 120, 745 (1960).

[43] J. Yamashita, T. Kurosawa, J. Phys. Chem. Solids 5, 34 (1958).

[44] T. Holstein, Ann. Phys 8, 325 (1959).

[45] K. Fesser, A. R. Bishop, D. K. Campbell, Phys. Rev. B 27, 4804 (1983).

[46] R. A. Marcus, J. Chem. Phys. 81, 4494 (1984).

[47] R. A. Marcus, N. Sutin, Biochim. Biophys. Acta 811, 265 (1985).

[48] K. Seki, M. Tachiya, Phys. Rev. B 65, 14305 (2001).

[49] P. G. Le Comber, W. E. Spear, Phys. Rev. Lett. 25, 509 (1970).

[50] G. Horowitz, R. Hajlaoui, P. Delannoy, J. Phys. III France 5, 355 (1995).

[51] Z. Bao, A. Dodubalapur, A.J. Lovinge, (1996).

[52] H. Sirringhans, P.J. Brown, R.H. Friend, M.M. Nielsen, K. Beckgrand, B.M.W. Langeveld-Voss, A. Spiering, R.A.J. Janssen, E.W. Meijer, P. Hermig. Nature , 401, 685 (1999).

[53] J.T. Bell, G.T. Mola, "Enhanced Current in P3HT/PCBM Bulk-Hetrojunction Solar cell", University of KwaZulu-Natal, Pietermaritzburg Campus, Private Bag X01, Scottsville 3209, South Africa. (unpublished)(2013).

[54] A.J. Moul, J.B. Bonekamp, and K. Meerholza, J. APPLIED PHYSICS 100, 094503 (2006).

Chapter 9

Appendices

The table below shows average efficiency and fill factor for all samples prepared in the laboratory. The sample parameters recorded here are for the samples prepared from the 26 November 2012 when I was starting with the laboratory work and 11 June 2013 when I was ending with the laboratory work. The devices prepared and tested were enough to do the analyses and conclude.

Sample	Fill Factor %	Efficiency %	RPM	Date
1	31	0.38	1000	26-11-2012
2	40	1.13	1300	19-11-2012
3	34	0.88	1500	30-11-2012
4	49	0.67	1200	12-12-2012

Table 9.1: Average efficiency and fill factor for all sample prepared

Sample	Fill Factor %	Efficiency %	RPM	Date
5	47	0.63	1500	12-12-2012
6	38	1.41	1300	13-12-2012
7	37	0.75	1560	13-12-2012
8	16	0.01	1300	11-01-2013
9	17	0.001	1500	11-01-2013
10	35	0.43	1500	18-02-2013
11	26	0.02	1300	11-01-2013
12	40	0.20	1300	18-02-2013
13	18	0.16	1420	19-02-2013
14	29	0.17	1600	19-02-2013
A1	45	0.46	1000	28-05-2012
A2	36	0.36	1260	28-05-2013
A3	33	0.10	1260	28-05-2013
B1	45	0.40	1300	29-05-2013
B2	13	0.01	1300	29-05-2013
C2	28	1.09	1100	30-05-2013
C3	23	0.54	1300	30-05-2013
C4	16	0.31	1300	30-05-2013
D1	20	0.01	1300	01-05-2013
D2	43	0.001	1300	01-05-2013
E1	29	2.0	1300	11-06-2013
E2	27	1.1	1300	11-06-2013
E3	46	4.2	1300	11-06-2013
E4	47	3.5	1300	11-06-2013

Table 9.2: Average efficiency and fill factor for all sample prepared